A mixed finite element method for curve diffusion flow using a biorthogonal system

Noura Alhawiti[1] Bishnu P. Lamichhane[2]
James McCoy[3]

(Received 29 January 2025; revised 8 August 2025)

Abstract

Finite element methods for higher order parabolic curve flow are reasonably well established since the pioneering work of Dzuik, Kuwert and Schätzle [SIAM J. Math. Anal., 33(5):1228–1245, 2002]. We develop here a new finite element scheme for a corresponding system of two second order equations for the curve diffusion flow using a biorthogonal system. This approach improves accuracy and efficiency over other methods.

Contents

DOI:10.21914/anziamproc.v66.19581 Published 2025-12-08, as part of the Proceedings of the 21st Biennial Computational Techniques and Applications Conference. ISSN 1445-8810. (Print two pages per sheet of paper.)

1 Introduction

Curve diffusion flow is a specific evolution law that governs how a curve changes shape over time. This law was introduced in 1956 by Mullins [7], who provided the first description of surface diffusion flow as a model for the formation of grooving at the grain boundaries of heated crystal structures. Fundamental theoretical and numerical results for the curve diffusion flow of closed curves were obtained by Dziuk et al. [4]. They developed numerical algorithms for both the curve diffusion equation and the related elastic flow. Their methods involve spatial discretisations using piecewise linear finite elements. The fourth order equation is converted to a natural system of two second order equations, the second being simply the formula for the curvature of the curve in terms of derivatives of its position vector. The semi-discrete system of two equations is then discretised in time using backward differences. Thus a system of linear equations can be solved at each time step.

Here we make an adjustment to the ideas of Dziuk et al. [4] by using a biorthogonal system with different finite element spaces for each of the two equations that simplify the calculations. Such an idea was used by Lamichhane [6], for example. More recently, for different boundary conditions for higher order linear and nonlinear equations, Das et al. [1] introduced a unified mixed finite element method for fourth order time-dependent problems using biorthogonal basis functions.

In terms of computational complexity for curve diffusion, our method in

Section 2 yields a very simple equation. We expect that for more complex flows, such as elastic flow, which involves more terms, the system derived using the biorthogonal approach will still be advantageous.

Section 3 verifies our computational technique by comparing numerical solutions with some known explicit closed curve solutions to the curve diffusion flow [5]. We also demonstrate an ellipse evolving to a circle as expected, although there is no explicit solution formula in this case.

2 Curve diffusion flow

A time-dependent family of curves $u : (a, b) \times (0, T] \to \mathbb{R}^2$ satisfies the curve diffusion flow defined by

$$\frac{\partial u}{\partial t} = -\frac{\partial^2 \kappa}{\partial s^2},$$

where κ denotes the curvature of u, and s is the arc length. Since κ is given precisely by the second arc length derivative of u, the curve diffusion is written as the system

$$\frac{\partial u}{\partial t} + \frac{\partial^2 \kappa}{\partial s^2} = 0, \quad (x, t) \in (a, b) \times (0, T], \tag{1}$$

$$\kappa - \frac{\partial^2 u}{\partial s^2} = 0, \quad (x, t) \in (a, b) \times (0, T]. \tag{2}$$

The first equation is fourth order, given the relationship between κ and u. However, (1–2) is an equivalent system of two second order equations, which is convenient for our approach. In our setting the variable $x \in (a, b)$ is identified with a point on the unit circle as we wish to consider closed curves; equivalently, $u(\cdot, t)$ will be periodic for every t.

We restrict this article to planar curves so $u(x, t) = (u_1(x, t), u_2(x, t)) \in \mathbb{R}^2$. The arc length of curve u, from starting point $u(a)$, is defined as

$$s(x, t) = \int_a^x \left| \frac{\partial u}{\partial x}(\tilde{x}, t) \right| d\tilde{x},$$

from which it follows that

$$\frac{\partial s}{\partial x}(x,t) = \left|\frac{\partial u}{\partial x}(x,t)\right|,$$

the length of the tangent vector in the x parametrisation.

2.1 The mixed formulation

We introduce an additional unknown variable ω that is the second derivative of the curvature with respect to arc length and therefore, from equation (2),

$$\omega = \frac{\partial^4 u}{\partial s^4}. \tag{3}$$

The main reason to introduce a new variable ω is to reduce the order of derivatives in the original PDE. As Lamichhane [6] shows, for example, equation (3) can be written as the energy functional minimization

$$\min_{(u,\psi)\in H^2(0,L)\times L^2(0,L)} \frac{1}{2}\int_0^L \psi^2\,ds - \int_0^L \omega u\,ds,$$

subject to

$$\psi = \frac{\partial^2 u}{\partial s^2}, \tag{4}$$

where H^k denotes the Sobolev space with kth order weak derivatives in L^2. Here L^2 is the classical Lebesgue space of square integrable functions. We refer to Wick [9] for more information on the spaces used here.

Multiplying (4) by a Lagrange multiplier $\mu(s)$, and integrating by parts, we get

$$\int_0^L \psi\mu\,ds = -\int_0^L \frac{\partial u}{\partial s}\frac{d\mu}{ds}\,ds, \quad \mu \in H^1(0,L).$$

The minimization problem is recast as a variational problem

$$\min_{(u,\psi)\in Q} \frac{1}{2}\int_0^L \psi^2\,ds - \int_0^L \omega u\,ds,$$

where $Q = H^1(0, L) \times L^2(0, L)$, and subject to

$$\int_0^L \psi\mu \, ds + \int_0^L \frac{\partial u}{\partial s}\frac{d\mu}{ds} \, ds = 0, \quad \mu \in H^1(0, L).$$

Constructing and computing the Lagrange equation, our problem becomes

$$\int_0^L \psi\varphi \, ds + \int_0^L \varphi\lambda \, ds + \int_0^L \frac{d\lambda}{ds}\frac{d\nu}{ds} \, ds = \int_0^L \omega\nu \, ds, \quad (\nu, \varphi) \in Q, \tag{5}$$

subject to

$$\int_0^L \psi\mu \, ds + \int_0^L \frac{\partial u}{\partial s}\frac{d\mu}{ds} \, ds = 0, \quad \mu \in H^1(0, L).$$

Now, getting back to equation (1), substituting $\omega = \partial^4 u/\partial s^4$, multiplying it by the test function ν and integrating over the domain gives us

$$\int_0^L \frac{\partial u}{\partial t}\nu \, ds + \int_0^L \omega\nu \, ds = 0, \tag{6}$$

for all test functions $\nu \in H^1(0, L)$. Substituting equation (5) into (6), the problem is to find $(u, \psi, \lambda) : (0, T] \to H^1(0, L) \times L^2(0, L) \times H^1(0, L)$ such that

$$\int_0^L \frac{\partial u}{\partial t}\nu \, ds + \int_0^L \psi\varphi \, ds + \int_0^L \lambda\varphi \, ds + \int_0^L \frac{d\lambda}{ds}\frac{d\nu}{ds} \, ds = 0, \quad (\nu, \varphi) \in Q, \tag{7}$$

subject to

$$\int_0^L \psi\mu \, ds + \int_0^L \frac{\partial u}{\partial s}\frac{d\mu}{ds} \, ds = 0, \quad \mu \in H^1(0, L).$$

Choosing the test functions $\varphi = 0$ and $\nu = 0$ in turn in equation (7) yields

$$\int_0^L \frac{\partial u}{\partial t}\nu \, ds + \int_0^L \frac{d\lambda}{ds}\frac{d\nu}{ds} \, ds = 0, \quad \text{for all } \nu \in H^1(0, L),$$
$$\int_0^L \psi\varphi \, ds + \int_0^L \lambda\varphi \, ds = 0, \quad \text{for all } \varphi \in L^2(0, L), \tag{8}$$

subject to

$$\int_0^L \psi\mu \, ds + \int_0^L \frac{\partial u}{\partial s}\frac{d\mu}{ds} \, ds = 0, \quad \mu \in H^1(0, L). \tag{9}$$

2.2 Finite element discretisations

We consider the discretisation of a nonlinear parabolic equation model in both space and time. Piecewise linear finite elements are used to discretise space, and later on, the backward Euler method is used to discretise time. Since $ds = |\partial u/\partial x|\,dx$ we convert (8) and (9) back into the standard x parametrisation to obtain

$$\int_a^b \frac{\partial u}{\partial t}\nu \left|\frac{\partial u}{\partial x}\right| dx + \int_a^b \frac{d\lambda}{dx}\frac{d\nu}{dx}\left|\frac{\partial u}{\partial x}\right|^{-1} dx = 0\,, \quad \text{for all } \nu \in H^1(a,b)\,,$$
$$\int_a^b \psi\varphi \left|\frac{\partial u}{\partial x}\right| dx + \int_a^b \lambda\varphi \left|\frac{\partial u}{\partial x}\right| dx = 0\,, \quad \text{for all } \varphi \in L^2(a,b)\,, \tag{10}$$

subject to

$$\int_a^b \psi\mu \left|\frac{\partial u}{\partial x}\right| dx + \int_a^b \frac{\partial u}{\partial x}\frac{d\mu}{dx}\left|\frac{\partial u}{\partial x}\right|^{-1} dx = 0\,, \quad \mu \in H^1(a,b)\,, \tag{11}$$

where $u, \lambda \in H^1(a,b)$, and ψ belongs to the biorthogonal space $\mathcal{M}(a,b) \subset L^2$. The advantage of this formulation is that the x variable (unlike s) is completely independent of t.

2.3 Construction of spaces

Consider a partition of the spatial interval $I = [a,b]$ into N equal parts such that

$$[a,b] = \bigcup_{j=1}^{N} I_j\,,$$

where $I_j = [x_{j-1}, x_j]$ for $1 \le j \le N$. Here I_j is called an element, $\{a = x_0, x_1, \ldots, x_N = b\}$ are the nodes (points), and $x_j = j\,\Delta x + x_0$ where $\Delta x_j = x_j - x_{j-1}$, and $\Delta x = \max_{1\le j\le N} \Delta x_j$ which is the spatial domain step size. We replace the continuous space, here $X = H^1(\mathbb{R}/\mathbb{Z} = I, \mathbb{R}^2)$ of periodic functions, with finite-dimensional subspaces by constructing suitable bases as

$$X_h = \{w \in C^0(I, \mathbb{R}^2) : w|_{I_j} \in \mathcal{P}_1(I_j), 1 \le j \le N\}\,.$$

Here X_h is a space of piecewise affine periodic functions; these functions are independent of time, and $\mathcal{P}_1(I_j)$ is the space of continuous polynomials of degree one on I_j.

Let $\nu_j(x)$ and $\mu_j(x)$ be suitable basis functions for $X_h(a,b) \subset H^1(a,b)$, and let $\varphi_j(x)$ be suitable basis functions in $\mathcal{M}_h(a,b)$. Our approximate solutions have the form

$$\begin{aligned} u_h(x,t) &= \sum_{j=1}^{N} u_j(t)\nu_j(x)\,, \\ \psi_h(x,t) &= \sum_{j=1}^{N} \psi_j(t)\varphi_j(x)\,, \\ \lambda_h(x,t) &= \sum_{j=1}^{N} \lambda_j(t)\mu_j(x)\,, \end{aligned} \tag{12}$$

where $\nu_j(x) = \mu_j(x)$ are the finite element basis functions, and $\mathcal{M}_h(a,b) \subset L^2(a,b)$ where $\mathcal{M}_h(a,b) = \{\varphi_j(x) \in L^2(a,b) : \varphi|_{I_j} \in \mathcal{P}_1(I_j), 1 \le j \le N\}$ and is biorthogonal to the standard basis function $\mu_j(x)$. The basis functions for $\mathcal{M}_h$ are

$$\varphi_j(x) = \begin{cases} \frac{2(x-x_{j-1})+(x-x_j)}{x_j-x_{j-1}} & \text{if } x_{j-1} \le x \le x_j\,, \\ \frac{2(x-x_{j+1})+(x-x_j)}{x_j-x_{j+1}} & \text{if } x_j \le x \le x_{j+1}\,, \\ 0 & \text{otherwise.} \end{cases}$$

Biorthogonal basis functions comprise two sets of basis functions $\{\mu_i\}_{i=1}^N$, and $\{\varphi_j\}_{j=1}^N$ that satisfy the biorthogonality condition. This means that $\int_a^b \mu_i\varphi_j\,dx = C_j\delta_{i,j}$ for constants $C_j > 0$ [6]. Here $\delta_{i,j}$ is the Kronecker delta.

The time dependence is completely through the time-dependent coefficient functions of the spatial basis functions. Substituting (12) into (10) and (11) we get

$$\int_a^b \frac{\partial u_h}{\partial t}\nu_h \left|\frac{\partial u_h}{\partial x}\right| dx + \int_a^b \frac{d\lambda_h}{dx}\frac{d\nu_h}{dx}\left|\frac{\partial u_h}{\partial x}\right|^{-1} dx = 0\,, \quad \text{for all } \nu_h \in X_h(a,b)\,,$$

$$\int_a^b \psi_h \varphi_h \left|\frac{\partial u_h}{\partial x}\right| dx + \int_a^b \lambda_h \varphi_h \left|\frac{\partial u_h}{\partial x}\right| dx = 0\,, \quad \text{for all } \varphi_h \in \mathcal{M}_h(a,b)\,, \tag{13}$$

subject to

$$\int_a^b \psi_h \mu_h \left|\frac{\partial u_h}{\partial x}\right| dx + \int_a^b \frac{\partial u_h}{\partial x}\frac{d\mu_h}{dx}\left|\frac{\partial u_h}{\partial x}\right|^{-1} dx = 0\,, \quad \mu_h \in X_h(a,b)\,. \tag{14}$$

Thus, the weak formulations (13), and (14) after calculating the integrals, give rise to the system

$$\begin{aligned}
&\tfrac{1}{2}\left(|u_j - u_{j-1}| + |u_{j+1} - u_j|\right)\frac{du_j(t)}{dt} - \frac{1}{|u_j - u_{j-1}|}\lambda_{j-1}(t)\\
&\quad + \frac{1}{|u_j - u_{j-1}| + |u_{j+1} - u_j|}\lambda_j(t) - \frac{1}{|u_{j+1} - u_j|}\lambda_{j+1}(t) = 0\,,\\
&-\tfrac{1}{2}|u_j - u_{j-1}|\,\psi_{j-1}(t) + \left(|u_j - u_{j-1}| + |u_{j+1} - u_j|\right)\psi_j(t)\\
&-\tfrac{1}{2}|u_{j+1} - u_j|\,\psi_{j+1}(t) + \tfrac{1}{2}\left(|u_j - u_{j-1}| + |u_{j+1} - u_j|\right)\lambda_j(t) = 0\,,
\end{aligned} \tag{15}$$

subject to

$$\begin{aligned}
&\tfrac{1}{2}\left(|u_j - u_{j-1}| + |u_{j+1} - u_j|\right)\psi_j(t) - \frac{1}{|u_j - u_{j-1}|}u_{j-1}(t)\\
&\quad + \frac{1}{|u_j - u_{j-1}| + |u_{j+1} - u_j|}u_j(t) - \frac{1}{|u_{j+1} - u_j|}u_{j+1}(t) = 0\,.
\end{aligned} \tag{16}$$

The scheme (15) and (16) has been discretised for time in a semi-implicit way, which is similar to the time discretisation used for the curve shortening flow in isotropic or anisotropic and evolution equation form [2, 3, 4]. Let $0 = t_1 < t_2 < \cdots < t_m = T$ be a partitioning of the time domain, and let $u_\ell \approx u(t_\ell)$ with $\ell = 1, \ldots, m$. We replace the time derivative by using the backward Euler method. Define the absolute quantities $h_j^\ell = \left|u_j^\ell - u_{j-1}^\ell\right|$

and $h_{j+1}^{\ell} = \left|u_{j+1}^{\ell} - u_j^{\ell}\right|$. Substituting the backward Euler method and the absolute quantities into (15) and (16), we get the linear system

$$\frac{1}{2}(h_j^{\ell} + h_{j+1}^{\ell})\frac{u_j^{\ell+1} - u_j^{\ell}}{\Delta t} - \frac{1}{h_j^{\ell}}\lambda_{j-1}^{\ell+1} + \frac{1}{h_j^{\ell} + h_{j+1}^{\ell}}\lambda_j^{\ell+1} - \frac{1}{h_{j+1}^{\ell}}\lambda_{j+1}^{\ell+1} = 0,$$
$$-\frac{1}{2}h_j^{\ell}\psi_{j-1}^{\ell+1} + (h_j^{\ell} + h_{j+1}^{\ell})\psi_j^{\ell+1} - \frac{1}{2}h_{j+1}^{\ell}\psi_{j+1}^{\ell+1} + \frac{1}{2}(h_j^{\ell} + h_{j+1}^{\ell})\lambda_j^{\ell+1} = 0,$$

subject to

$$\frac{1}{2}(h_j^{\ell} + h_{j+1}^{\ell})\psi_j^{\ell+1} - \frac{1}{h_j^{\ell}}u_{j-1}^{\ell+1} + \frac{1}{h_j^{\ell} + h_{j+1}^{\ell}}u_j^{\ell+1} - \frac{1}{h_{j+1}^{\ell}}u_{j+1}^{\ell+1} = 0,$$

for $\ell = 1, \ldots, m$, with the periodic boundary condition $u_i = u_{i+N}$ with $i \in \mathbb{Z}$ and the initial values $u_j(0) = u_0(x_j)$ with $j = 1, \ldots, N$.

We need to solve the linear system

$$D_{\ell}u^{\ell+1} + \Delta t A_{\ell}\lambda^{\ell+1} = D_{\ell}u^{\ell},$$
$$\tilde{M}_{\ell}\psi^{\ell+1} + D_{\ell}\lambda^{\ell+1} = 0,$$

subject to

$$D_{\ell}\psi^{\ell+1} + A_{\ell}u^{\ell+1} = 0,$$

where the diagonal and two tridiagonal matrices are, respectively,

$$D_{\ell} = \begin{bmatrix} \frac{1}{2}(h_j^{\ell} + h_{j+1}^{\ell}) & 0 & \cdots & 0 \\ 0 & \ddots & \ddots & \vdots \\ \vdots & \ddots & \ddots & 0 \\ 0 & \cdots & 0 & \frac{1}{2}(h_j^{\ell} + h_{j+1}^{\ell}) \end{bmatrix},$$

$$A_{\ell} = \begin{bmatrix} \frac{1}{h_j^{\ell}} + \frac{1}{h_{j+1}^{\ell}} & -\frac{1}{h_{j+1}^{\ell}} & 0 & \cdots & 0 \\ -\frac{1}{h_j^{\ell}} & \ddots & \ddots & \ddots & \vdots \\ 0 & \ddots & \ddots & \ddots & 0 \\ \vdots & \ddots & \ddots & \ddots & -\frac{1}{h_j^{\ell}} \\ 0 & \cdots & 0 & -\frac{1}{h_j^{\ell}} & \frac{1}{h_j^{\ell}} + \frac{1}{h_{j+1}^{\ell}} \end{bmatrix},$$

$$\tilde{M}_\ell = \begin{bmatrix} h_j^\ell + h_{j+1}^\ell & -\frac{1}{2}h_{j+1}^\ell & 0 & \cdots & 0 \\ -\frac{1}{2}h_j^\ell & \ddots & \ddots & \ddots & \vdots \\ 0 & \ddots & \ddots & \ddots & 0 \\ \vdots & \ddots & \ddots & \ddots & -\frac{1}{2}h_{j+1}^\ell \\ 0 & \cdots & 0 & -\frac{1}{2}h_j^\ell & h_j^\ell + h_{j+1}^\ell \end{bmatrix}$$

These matrices depend on the results of the previous time step. By substituting the λ and ψ into the equation system we arrive at

$$\left[D_\ell + \Delta t\, A_\ell^T\, (D_\ell^{-1})^T \tilde{M}_\ell\, D_\ell^{-1} A_\ell\right] \vec{u}^{\ell+1} = D_\ell \vec{u}^\ell\,. \tag{17}$$

Furthermore, the curvature can be found from equation (2) using the direct finite element method. Multiplying equation (2) by a test function ν and integrating over the domain gives us

$$\int_0^L \kappa\nu\, ds + \int_0^L \frac{\partial u}{\partial s}\frac{d\nu}{ds}\, ds = 0\,, \quad \text{for all } \nu \in H^1(0, L)\,. \tag{18}$$

The standard form for equation (18) is

$$\int_a^b \kappa\nu \left|\frac{\partial \kappa}{\partial x}\right| dx + \int_a^b \frac{\partial u}{\partial x}\frac{d\nu}{dx}\left|\frac{\partial u}{\partial x}\right|^{-1} dx = 0\,, \quad \text{for all } \nu \in H^1(a, b)\,. \tag{19}$$

Taking a basis $\{\nu_j(x)\}_1^N$ of $X_h(a, b)$ for $\kappa \in H^1(a, b)$, the discrete solution for κ is

$$\kappa_h(x, t) = \sum_{j=1}^{N} \kappa_j(t)\, \nu_j(x)\,.$$

Substituting the discrete solutions into (19) and calculating integrals lead to

$$\vec{\kappa}^{\ell+1} = -D_\ell^{-1} A_\ell \vec{u}^{\ell+1}\,. \tag{20}$$

Equation (20) needs to be calculated for each time step $\ell = 1, \ldots, m$, with periodic boundary condition $\kappa_i = \kappa_{i+N}$ with $i \in \mathbb{Z}$ and initial values $\kappa_j(0) = \kappa_0(x_j)$.

Table 1: Errors for the function u for the circle under diffusion flow.

N	Max error	Max rate	L^2 error	L^2 rate	H^1 error	H^1 rate
10	9.84e-01	-	1.74	-	2.40	-
20	6.30e-01	0.6442	1.12	0.6442	1.57	0.6157
40	2.19e-01	1.5255	3.88e-01	1.5255	5.47e-01	1.5174
80	5.98e-02	1.8706	1.06e-01	1.8706	1.50e-01	1.8685
160	1.53e-02	1.9668	2.71e-02	1.9668	3.84e-02	1.9662
320	3.85e-03	1.9916	6.82e-03	1.9916	9.64e-03	1.9915
640	9.63e-04	1.9979	1.71-03	1.9979	2.41e-03	1.9979
1280	2.41e-04	1.9995	4.27e-04	1.9995	6.04e-04	1.9995
2560	6.02e-05	1.9999	1.07e-04	1.9999	1.51e-04	1.9999
5120	1.51e-05	2.0000	2.67e-05	2.0000	3.77e-05	2.0000

3 Numerical experiments

In this section, we present some numerical tests to gauge the performance of our algorithm. We compute the maximum error using the L^∞-norm, L^2-error using the L^2-norm, and H^1-error using the H^1-norm. The convergence rates of these norms are also presented. We observe convergence rates of almost two for all these norms.

As a first example we consider a circle $u_0(x) = (\cos x, \sin x)$ which is stationary under the curve diffusion flow. Both the exact solution and our numerical approximation remain stationary, as shown in Figure 1, while the errors of u and κ are shown in Table 1 and Table 2, respectively.

For our second example, we consider a known explicit solution to the curve diffusion flow [5], namely the shrinking figure eight with

$$u(x,t) = \frac{(1-24\,t)^{\frac{1}{4}}}{1+\sin^2 x}(\cos x, \cos x \sin x)\,,$$

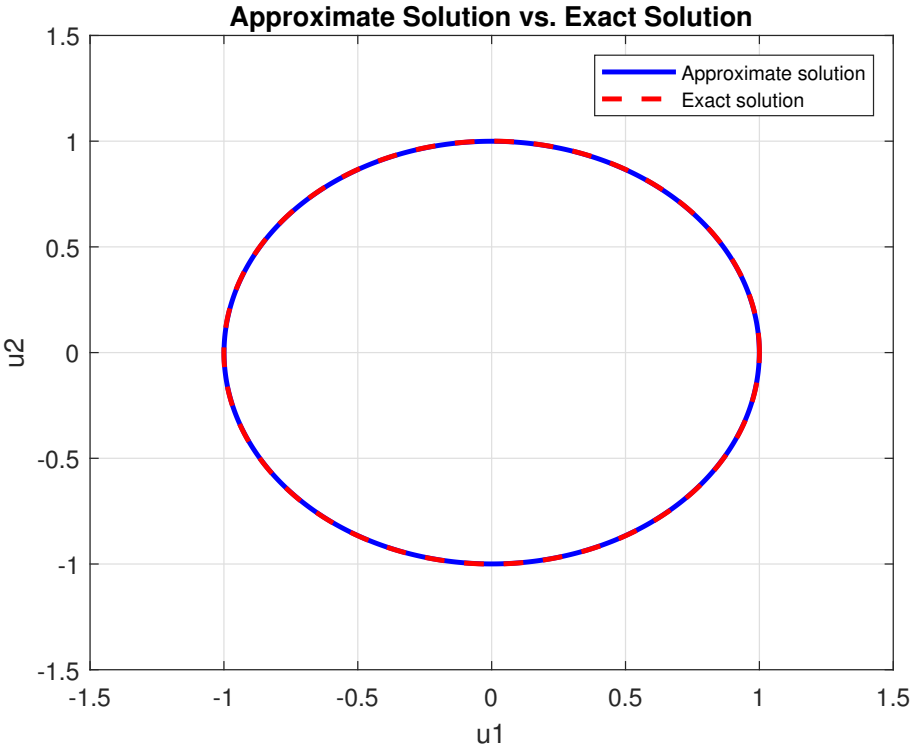

Figure 1: The approximate and exact solutions of the curve diffusion flow for a closed curve with an initial circle.

Table 2: Errors for the curvature κ for the circle under diffusion flow.

N	Max error	Max rate	L^2 error	L^2 rate	H^1 error	H^1 rate
10	9.84e-01	-	1.74	-	2.40	-
20	6.30e-01	0.6442	1.12	0.6442	1.57	0.6157
40	2.19e-01	1.5255	3.88e-01	1.5255	5.47e-01	1.5174
80	5.98e-02	1.8706	1.06e-01	1.8706	1.50e-01	1.8685
160	1.53e-02	1.9668	2.71e-02	1.9668	3.84e-02	1.9662
320	3.85e-03	1.9916	6.82e-03	1.9916	9.64e-03	1.9915
640	9.63e-04	1.9979	1.71e-03	1.9979	2.41e-03	1.9979
1280	2.41e-04	1.9995	4.27e-04	1.9995	6.04e-04	1.9995
2560	6.02e-05	1.9999	1.07e-04	1.9999	1.51e-04	1.9999
5120	1.51e-05	2.0000	2.67e-05	2.0000	3.77e-05	2.0000

where it is straightforward to calculate

$$\kappa(x,t) = \frac{(1-24t)^{-\frac{1}{4}}}{(\cos^2 x - 2)^2}(3\cos x[3\sin^2 x - 1], 3\cos x \sin x[\sin^2 x - 3])\,,$$

as demonstrated by Edwards et al. [5]. The symmetry of the figure eight implies that the signed area is equal to zero and remains constant under flow. In our example, the numerical solution shrinks to a point at time $T = 1/24$. In our numerical approximation we take the same initial curve $u_0(x) = u(x,0)$ as given above. The results are shown in Figure 2, and the errors of u and κ are shown in Table 3 and Table 4, respectively.

As a final example, we consider the case of an evolving flower-shaped curve with initial curve $u_0(x) = ([3+\sin(5x)]\cos x, [3+\sin(5x)]\sin x)$, and an ellipse curve with an initial curve $u_0(x) = (2\cos x, \sin x)$. There are no explicit solutions for these curve diffusion flows with these initial curves, however, for very small 'petals' Wheeler [8] showed that the flow will drive this curve towards a circle enclosing the same area. Our numerical results suggest the conditions given by Wheeler are not strong: flowers with larger petals also appear to converge under curve diffusion flow to circles.

Table 3: Errors for the function $\mathfrak{u}$ for figure eight under diffusion flow.

N	Max error	Max rate	L^2 error	L^2 rate	H^1 error	H^1 rate
10	3.10e-01	-	6.63e-01	-	8.65e-01	-
20	1.08e-01	1.5234	1.80e-01	1.8032	4.73e-01	0.8711
40	4.15e-02	1.3804	7.08e-02	1.3423	2.24e-01	1.0789
80	1.40e-02	1.5661	2.04e-02	1.7974	7.46e-02	1.5845
160	3.90e-03	1.8422	5.38e-03	1.9225	2.12e-02	1.8160
320	1.02e-03	1.9331	1.37e-03	1.9767	5.52e-03	1.9413
640	2.59e-04	1.9808	3.43e-04	1.9938	1.40e-03	1.9840
1280	6.50e-05	1.9950	8.58e-05	1.9984	3.50e-04	1.9959
2560	1.63e-05	1.9987	2.15e-05	1.9996	8discretis.75e-05	1.9990
5120	4.07e-06	1.9997	5.37e-06	1.9999	2.19e-05	1.9998

Table 4: Errors for the curvature κ for figure eight under diffusion flow.

N	Max error	Max rate	L^2 error	L^2 rate	H^1 error	H^1 rate
10	5.09	-	6.72	-	1.31e+1	-
20	1.80	1.4962	2.43	1.4702	7.21	0.8630
40	8.97e-01	1.0074	1.05	1.2023	4.22	0.7735
80	3.59e-01	1.3209	3.90e-01	1.4349	1.86	1.1824
160	1.14e-01	1.6551	1.15e-01	1.7644	6.11e-01	1.6052
320	3.12e-02	1.8671	3.03e-02	1.9199	1.69e-01	1.8567
640	8.04e-03	1.9590	7.71e-03	1.9773	4.34e-02	1.9581
1280	2.03e-03	1.9865	1.94e-03	1.9925	1.09e-02	1.9880
2560	5.15e-04	1.9771	4.89e-04	1.9849	2.76e-03	1.9890
5120	1.43e-04	1.8481	1.34e-04	1.8707	7.24e-04	1.9298

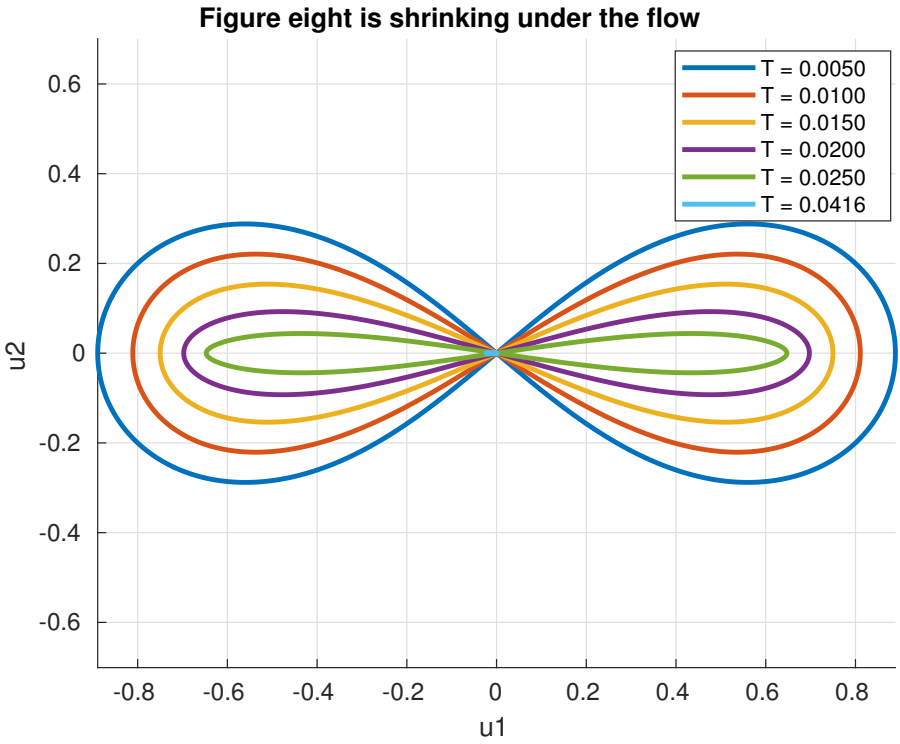

Figure 2: The diffusion flow curve for a figure eight at different times.

Discretisation methods often introduce numerical dissipation. This dissipation causes a loss of area, even if the theoretical system preserves it. For the flower-shaped curve, the initial area is 29.748667 and the final area is 27.260541, and for the ellipse curve, the initial area is 6.282152 and the final area is 4.798564, which are only slight differences, as shown in Figure 3 and Figure 4.

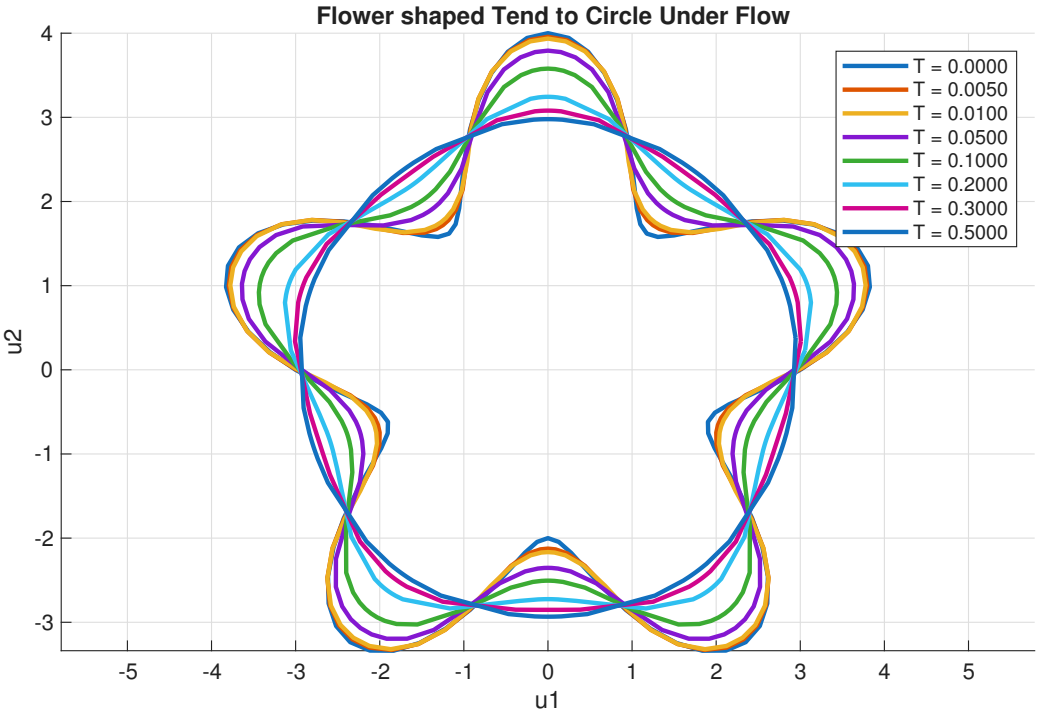

Figure 3: The diffusion flow for a flower-shape at different times.

4 Conclusion

We presented a mixed finite element method for the curve diffusion equation for evolving closed curves using a biorthogonal system. The structure of the biorthogonal system helps in simplifying computations for the numerical solution, providing a system that is easy to solve. The presented numerical results demonstrate the efficiency and accuracy of the approach. With the method here confirmed as accurate in several examples, it is now appropriate to investigate its behaviour in settings where singularities occur.

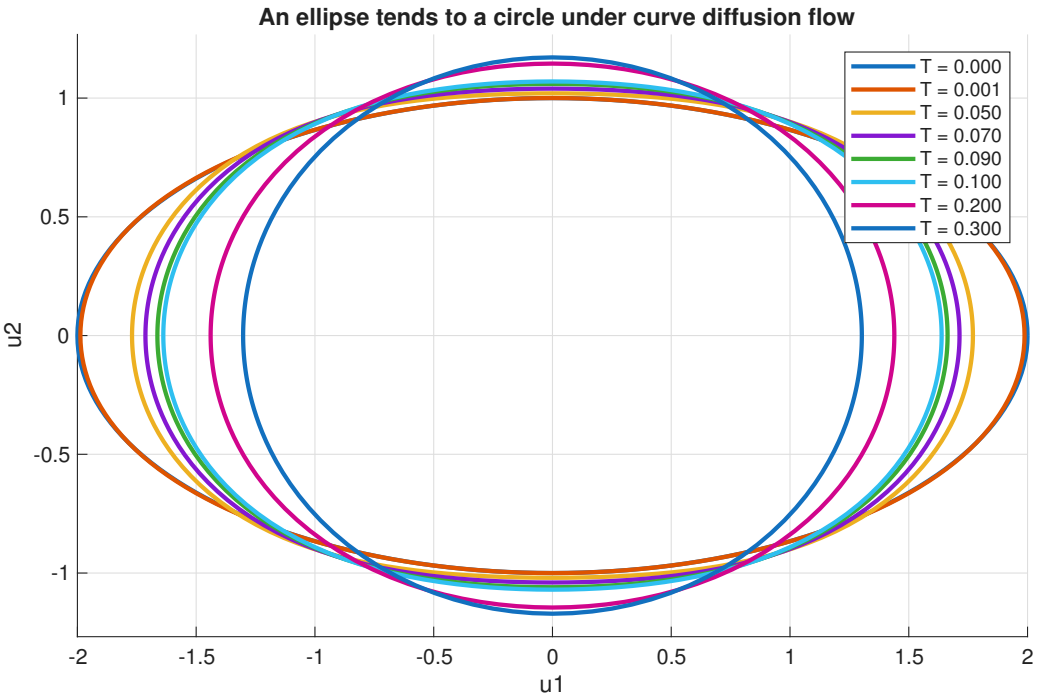

Figure 4: The diffusion flow for an ellipse at different times.

Acknowledgements Part of this work was completed while the third author was visiting the University of Science and Technology, China, supported by a Chinese Academy of Sciences President's International Fellowship Initiative visiting fellowship, Grant number 2024PVA0042. The first author acknowledges the University of Tabuk for financial support under a postgraduate scholarship.

References

[1] A. Das, B. P. Lamichhane, and N. Nataraj. "A unified mixed finite element method for fourth-order time-dependent problems using

biorthogonal systems". In: *Comput. Math. Appl.* 165 (2024), pp. 52–69. DOI: 10.1016/j.camwa.2024.04.013 (cit. on p. C2).

[2] G. Dziuk. "Convergence of a semi-discrete scheme for the curve shortening flow". In: *Math. Mod. Meth. Appl. Sci.* 4.04 (1994), pp. 589–606. DOI: 10.1142/S0218202594000339 (cit. on p. C8).

[3] G. Dziuk. "Discrete anisotropic curve shortening flow". In: *SIAM J. Num. Anal.* 36.6 (1999), pp. 1808–1830. DOI: 10.1137/S0036142998337533 (cit. on p. C8).

[4] G. Dziuk, E. Kuwert, and R. Schätzle. "Evolution of elastic curves in \Rn: Existence and computation". In: *SIAM J. Math. Anal.* 33.5 (2002), pp. 1228–1245. DOI: 10.1137/S0036141001383709 (cit. on pp. C2, C8).

[5] M. Edwards, A. Gerhardt-Bourke, J. McCoy, G. Wheeler, and V.-M. Wheeler. "The shrinking figure eight and other solitons for the curve diffusion flow". In: *The mechanics of ribbons and Möbius bands.* Ed. by R. Fosdick and E. Fried. Dordrecht: Springer Netherlands, 2016, pp. 191–211. DOI: 10.1007/978-94-017-7300-3_11 (cit. on pp. C3, C11, C13).

[6] B. P Lamichhane. "A mixed finite element method for the biharmonic problem using biorthogonal or quasi-biorthogonal systems". In: *J. Sci. Comput.* 46 (2011), pp. 379–396. DOI: 10.1007/s10915-010-9409-7 (cit. on pp. C2, C4, C7).

[7] W. W. Mullins. "Theory of thermal grooving". In: *J. Appl. Phys.* 28.3 (1957), pp. 333–339. DOI: 10.1063/1.1722742 (cit. on p. C2).

[8] G. Wheeler. "On the curve diffusion flow of closed plane curves". In: *Ann. Mat. Pura Appl.* 192.5 (2013), pp. 931–950. DOI: 10.1007/s10231-012-0253-2 (cit. on p. C13).

[9] T. Wick. "Numerical methods for partial differential equations". In: Lecture notes. Institutionelles Repositorium der Leibniz Universität Hannover, 2022. DOI: 10.15488/11709 (cit. on p. C4).

Author addresses

1. **Noura Alhawiti**, School of Information and Physical Sciences, Mathematics Building, University of Newcastle, University Drive, Callaghan, NSW 2308, Australia; and Department of Mathematics, Faculty of Science, University of Tabuk, Tabuk 71491, Saudi Arabia.
mailto:nourahamadm.alhawiti@uon.edu.au;nalhawiti@ut.edu.sa
orcid:0009-0001-4791-0699

2. **Bishnu P. Lamichhane**, School of Information and Physical Sciences, Mathematics Building, University of Newcastle, University Drive, Callaghan, NSW 2308, Australia.
mailto:Bishnu.Lamichhane@newcastle.edu.au
orcid:0000-0002-9184-8941

3. **James McCoy**, School of Information and Physical Sciences, Mathematics Building, University of Newcastle, University Drive, Callaghan, NSW 2308, Australia.
mailto:James.McCoy@newcastle.edu.au
orcid:0000-0001-6053-5144